Demodulation method for tilted fiber Bragg grating refractometer with high sensitivity

Xuantung Pham, Jinhai Si, Tao Chen, Ruize Wang, Lihe Yan, Houjun Cao, and Xun Hou

Citation: Journal of Applied Physics **123**, 174501 (2018); doi: 10.1063/1.5025645
View online: https://doi.org/10.1063/1.5025645
View Table of Contents: http://aip.scitation.org/toc/jap/123/17
Published by the American Institute of Physics

Demodulation method for tilted fiber Bragg grating refractometer with high sensitivity

Xuantung Pham,[1,2] Jinhai Si,[1,a)] Tao Chen,[1,3] Ruize Wang,[1] Lihe Yan,[1] Houjun Cao,[1] and Xun Hou[1]

[1]*Key Laboratory for Physical Electronics and Devices of the Ministry of Education and Shaanxi Key Lab of Information Photonic Technique, School of Electronics and Information Engineering, Xi'an Jiaotong University, No. 28, Xianning West Road, Xi'an 710049, China*
[2]*Le Quy Don Technical University, Hanoi 122314, Vietnam*
[3]*Xi'an Jiaotong University Suzhou Academy, Suzhou 215123, China*

(Received 11 February 2018; accepted 12 April 2018; published online 1 May 2018)

In this paper, we propose a demodulation method for refractive index (RI) sensing with tilted fiber Bragg gratings (TFBGs). It operates by monitoring the TFBG cladding mode resonance "cut-off wavelengths." The idea of a "cut-off wavelength" and its determination method are introduced. The RI sensitivities of TFBGs are significantly enhanced in certain RI ranges by using our demodulation method. The temperature-induced cross sensitivity is eliminated. We also demonstrate a parallel-double-angle TFBG (PDTFBG), in which two individual TFBGs are inscribed in the fiber core in parallel using a femtosecond laser and a phase mask. The RI sensing range of the PDTFBG is significantly broader than that of a conventional single-angle TFBG. In addition, its RI sensitivity can reach 1023.1 nm/refractive index unit in the 1.4401–1.4570 RI range when our proposed demodulation method is used. *Published by AIP Publishing*. https://doi.org/10.1063/1.5025645

I. INTRODUCTION

Tilted fiber Bragg gratings (TFBGs) inherit the useful characteristics of uniform fiber Bragg gratings (FBGs) and long period fiber gratings (LPFGs).[1,2] They have been studied extensively,[3–6] and are considered to be important optical fiber sensor components.[7–10] Due to their special structures, TFBGs enable light coupling not only between the forward and backward core modes, but also between the forward core mode, backward cladding modes, and even radiation modes.[3] Since their cladding modes can interact significantly with external environmental media, they have been used widely in field of surrounding refractive index (SRI) sensing.[11–13]

Two primary techniques have been proposed for SRI sensing using TFBGs. Zhou *et al.* presented a technique by which the absolute refractive index of surrounding media in the near-infrared region can be directly measured by using the resonance wavelength of the cut-off mode and the phase matching equation. This method produces an uncertainty of 10^{-3},[14] but more accurate results can be obtained using the exact wavelength positions of a large set of cladding mode resonances and a TFBG calibration model.[15] The second method is based on extracting SRI changes with respect to a well-known reference by correlating it with the evolution of the TFBG transmission spectrum. Thus far, several demodulation methods have been proposed based on this idea.[1,5,16–18] The first method proposed was based on global monitoring of the area delimited by the cladding and radiation mode resonances in the transmission spectrum. This is relatively insensitive to temperature and changes monotonically with SRI between 1.32 and 1.42.[1] The temperature-induced cross sensitivity can be completely eliminated by monitoring the selected cladding mode resonance shifts with respect to the Bragg wavelength.[16] The sensitivity is quite poor for low SRI values but increases dramatically as the SRI approaches the value at which the selected cladding mode is cut-off. Thus, the crux of this scheme is selecting the cladding mode that best enables high-sensitivity sensing of the appropriate SRI range. The cut-off mode is the boundary between the guided and leaky modes, and is evidenced by a cladding mode resonance amplitude that decreases as the SRI increases.[19] Because it exhibits higher refractive index (RI) sensitivity than other cladding modes, it has recently been used for SRI sensing.[13,20] The relationship between the cut-off mode resonance wavelength and the SRI is highly linear with a sensitivity of about 500 nm/refractive index unit (RIU). However, the process of locating the cut-off mode is relatively complex since it requires calculating the upper and lower envelopes of the transmission spectrum as well as these envelopes' normalized derivatives.[18]

A TFBG with a fixed tilt angle can be used for RI measurements only within a specific range. Thus, research has been performed in order to broaden the RI sensing range.[13,21] Chen *et al.* inscribed a multi-angle TFBG (MATFBG) consisting of five-concatenated TFBGs that was capable of RI measurement across a wide RI range of 1.15–1.45.[13] However, since the tilted gratings are produced by consistently rotating the phase mask and fiber (this also requires tilting the cylindrical lens that is used to focus the writing laser intensity along the fiber axis) around an axis perpendicular to the laser beam,[9,13] these components require various adjustment to match the tilt angles of the fabricated TFBGs. Consequently, the fabrication complexity increases. Recently, we proposed a simple method for TFBG fabrication,[22] in which the phase mask and cylindrical lens are

[a)]Electronic mail: jinhaisi@mail.xjtu.edu.cn

fixed. The scanning angle of the fiber that determines the TFBG tilt angle can be controlled using a computer program. However, due to the concatenated structure of the MATFBG, even though when our fabrication method is used, the fiber still requires a movement in a range of a few millimeters before each exposure (when each TFBG of the MATFBG is fabricated). The change in the relative positions of the fiber with respect to the phase mask and the focal line of the cylindrical lens can occur if the movable platform offers insufficient precision in that moving range. Hence, the fiber position may need to be aligned for each TFBG in the MATFBG.

In this paper, we propose a demodulation method based on monitoring the "cut-off wavelength" (CW) of the TFBG cladding mode resonances as a method of SRI measurement. The "cut-off wavelength" is obtained by using a relative transmission spectrum and a threshold value. Our demodulation method improves the TFBG RI sensitivity in a specific RI range, and enables elimination of temperature-induced cross sensitivity. We also fabricate a parallel-double-angle TFBG (PDTFBG), in which two individual TFBGs are written in the fiber core in parallel using femtosecond laser irradiation and the phase mask. The RI response of the PDTFBG is investigated and compared to those of conventional single-angle TFBGs (STFBGs). The PDTFBG effectively enhances the RI sensing range compared to a conventional STFBG.

II. EXPERIMENTAL METHOD

In our experiments, the PDTFBG and STFBG were written in a single-mode fiber (fiber core diameter ~9 μm) using a femtosecond laser and a phase mask. The schematic of the TFBG fabrication system is shown in Fig. 1(a).The

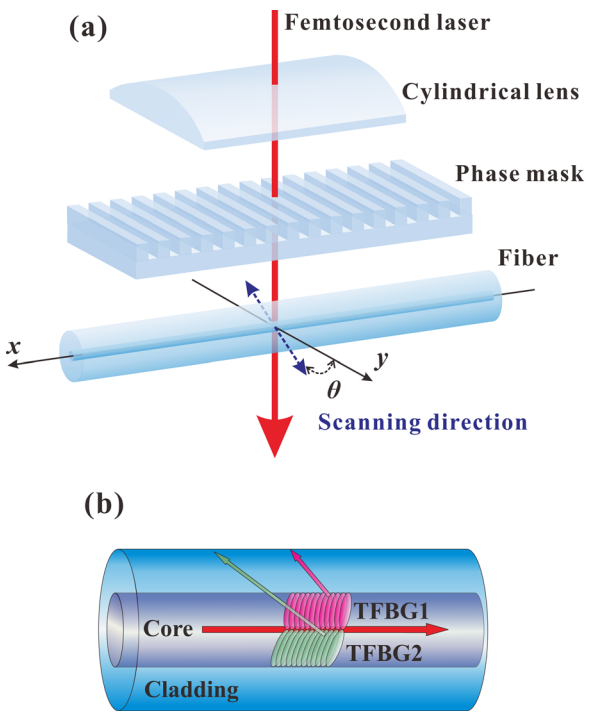

FIG. 1. (a) A schematic that shows fabrication of a TFBG using femtosecond laser irradiation with a phase mask. (b) Configuration of the grating distribution in the PDTFBG fiber core.

fabrication method that we proposed previously[22] was used to fabricate tilted grating planes in the fiber. According to this method, the scanning angle of the fiber that determines the TFBG tilt angle was achieved by simultaneously scanning the fiber across its x- and y-axes. Moreover, the scanning values of the fiber across its x- and y-axes could be controlled using a computer program. Hence, TFBGs with different tilt angles could be fabricated easily at different parts of the fiber by changing the fiber scanning parameters. A detailed description of the experimental apparatus is given in Ref. 22.

The PDTFBG structure is shown in Fig. 1(b). The PDTFBG consisted of two different TFBGs arranged in parallel with each other at the same position in the fiber core. Its fabrication process included three main steps. First, the relative positions of the fiber, phase mask, and cylindrical lens were adjusted precisely based on the TFBG fabrication parameters.[22] Then, the fiber scanning parameters for the x- and y-axes were set to the correct values for fabrication of TFBG1. The scanning range was limited to ensure that the grating region correctly covered the upper half of the fiber core. Finally, the TFBG2 was properly fabricated on the lower half of the fiber core by changing the fiber scanning parameters. Due to the parallel structure of the PDTFBG, readjusting the relative position of the fiber with respect to the phase mask and cylindrical lens before the fabrication of TFBG2 was not required. This reduces the fabrication process complexity. The fabrication method proposed in Ref. 22 ensures that the grating periods along the fiber axial direction of the TFBGs are independent of the fabricated tilt angles and that could be given by $\Lambda_g = \Lambda_m/2$, where Λ_m is the period of the phase mask.[22] Thus, the Bragg wavelengths of the different STFBGs and PDTFBGs are identical.

The fabricated PDTFBGs and STFBGs were used as a sample for SRI sensing experiments, and their RI responses were investigated by using our proposed demodulation method. A broadband amplified spontaneous emission (ASE) light source with a spectrum range of 1510–1570 nm was launched into these TFBGs, and their transmission spectra were recorded using an optical spectrum analyzer with a spectral resolution of 20 pm. During the SRI measurement, the temperature was kept at 23.5 °C. Aqueous glycerin solutions of various concentrations were used as the surrounding media and their refractive indices (RIs) were calibrated at a wavelength of 589.3 nm using an Abbe refractometer. Changing the aqueous glycerin solution concentration allowed its refractive index to be varied within the wide range of 1.3323–1.4716. To keep the strain on the fiber constant during the experiments, the TFBG grating region was permanently attached to a microscope slide, and small quantities of liquids with various refractive indices were dispensed onto the gratings via a pipette. Moreover, the grating regions and slides were cleaned thoroughly between experiments.

III. RESULTS AND DISCUSSION

A. Fabrication

Three STFBGs with tilt angles of 2.2°, 3.8°, and 6.3° were written using the fabrication method described in

Ref. 22. In the PDTFBG fabrication process, the fiber scanning value was set to 8 μm in the y-axis, and the value for the x-axis was set differently to produce a PDTFBG with two desired tilt angles.

Figure 2 shows optical microscopy images of two fabricated PDTFBGs, in which the tilt angles are 2.2°, 3.8°, and 2.2°, 14.9°, respectively. The two TFBGs in each PDTFBG are continuously inscribed in the transverse direction of the fiber core. Each TFBG in the PDTFBG is correctly written in the corresponding half of the fiber core, such that they even cover part of the fiber cladding. Their configurations can be distinct when the difference between the two tilt angles is sufficiently large, as shown in Fig. 2(b). The grating periods of all fabricated TFBGs are 1.07 μm along the fiber axial direction.

Figure 3 shows the measured transmission spectrum of the 2.2°, 3.8° PDTFBG and those of STFBGs with tilt angles of 2.2°, 3.8°, and 6.3°, respectively. The cladding mode resonance peak losses reach about –16 dB, –11 dB, –7.0 dB, and –9.9 dB with the 2.2° STFBG, 3.8° STFBG, 6.1° STFBG, and PDTFBG, respectively. When the STFBG tilt angle increases, the range of its cladding mode resonance increases, and the envelope of its cladding mode resonances shifts according to the short wavelength side. As a result, its RI sensing range can widen but shifts to a smaller RI region. Moreover, the resonance intensities of the Bragg and ghost modes decrease as the tilt angle increases. They completely disappear in the case of the 6.3° STFBG, as shown in Fig. 3. Since the Bragg wavelength is typically used as a reference to eliminate temperature-induced cross sensitivity in SRI sensing,[16,20] a temperature-insensitive SRI sensor can be difficult to produce by using the STFBG with a large tilt angle (for example the 6.3° STFBG). The cladding mode resonance range of the 2.2°, 3.8° PDTFBG is from 1510 nm to 1548 nm. That is even wider than the sum of the cladding mode resonance ranges of the 2.2° and 3.8° STFBGs. Two phenomena may contribute to these results. First, each

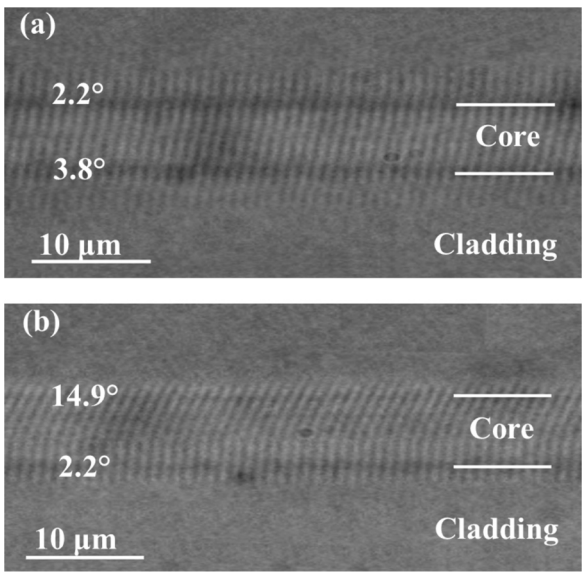

FIG. 2. Optical microscopy images of a PDTFBG with tilt angles of (a) 2.2° and 3.8° and (b) 14.9° and 2.2°.

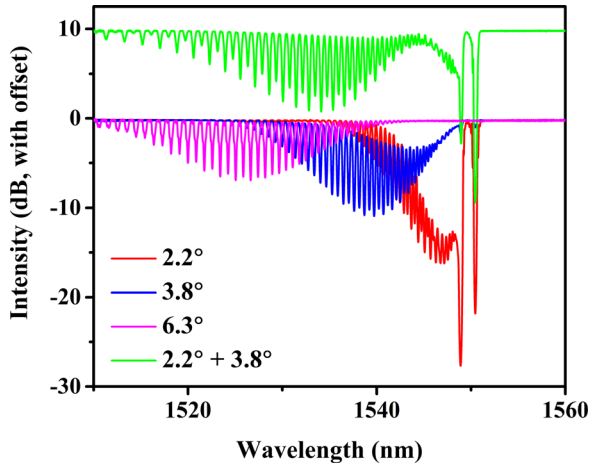

FIG. 3. An air transmission spectrum of a PDTFBG with tilt angles 2.2° and 3.8° and those of conventional STFBGs with tilt angles of 2.2°, 3.8°, and 6.3° (the spectra of the two types of TFBGs are offset by 10 dB for clarity).

TFBG of the PDTFBG can be considered as a special configuration of the off-axis FBG. This enhances coupling to cladding modes significantly.[23] Second, interactions can occur between portions of light that are coupled by the two TFBGs in the PDTFBG since they are parallel to each other. This may enhance light coupling to higher-order cladding modes, resulting in extension of the cladding mode resonance range. The spectra of these TFBGs show that the RI sensing range of the PDTFBG could be much wider than those of the 2.2° STFBG and 3.8° STFBG. Moreover, the Bragg mode of the 2.2°, 3.8° PDTFBG still remains with a resonance intensity of about –19 dB, which can be used to realize temperature-insensitive SRI sensing across a wide RI range.

B. Demodulation method for SRI sensing

Figure 4(a) shows variations in the 3.8° STFBG transmission spectra as measured in various RI solutions. The cladding mode resonances on the short wavelength side are gradually suppressed as the SRI increases. They completely vanish and the transmission spectrum becomes a smooth curve at an SRI of 1.4578. The basic idea of our new demodulation method is to use the smooth-curve transmission spectrum (when all cladding modes are completely suppressed) as a reference to calibrate the evolutions of TFBG transmission spectra in various RI solutions. TFBGs with different tilt angles may require different RI solutions to produce smooth-curve transmission spectra.

Our demodulation method can be divided into three main steps. First, we obtain the smooth-curve transmission spectrum by measuring TFBG transmission spectra at RI values that are approximately equal to that of the fiber cladding, and used it as the reference spectrum. Then, the relative transmission spectrum is obtained by subtracting the reference spectrum from the measured transmission spectrum of the TFBG. The relevant equation can be given as

$$T_{RS}^{dB}(\lambda) = T_{M}^{dB}(\lambda) - T_{R}^{dB}(\lambda) = 10\log\left(\frac{T_M(\lambda)}{T_R(\lambda)}\right), \quad (1)$$

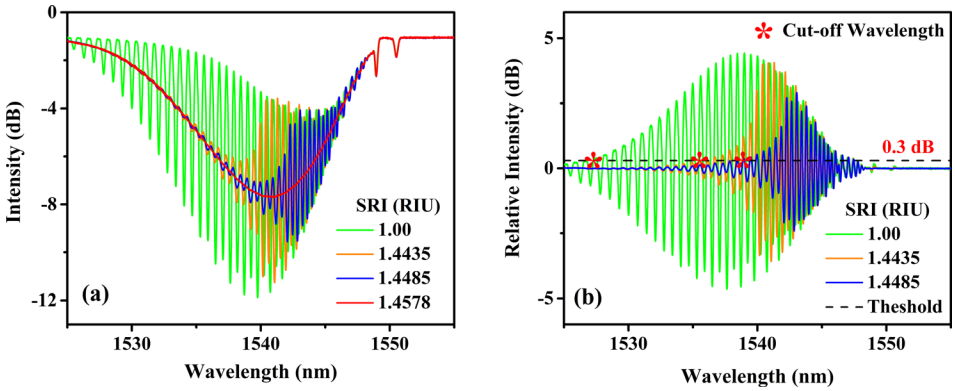

FIG. 4. (a) Variations in the transmission spectra of the 3.8° STFBG in different RI solutions, and (b) their corresponding relative transmission spectra when the transmission spectrum at the SRI of 1.4578 is used as a reference. The line at 0.3 dB is considered the threshold line for the cut-off wavelength (marked with red asterisks).

where $T_{RS}^{dB}(\lambda)$ is the relative transmission spectrum in decibel term, $T_{M}^{dB}(\lambda)$ *and* $T_M(\lambda)$ are the measured transmission spectrum in decibel and percentage terms, and $T_{R}^{dB}(\lambda)$ *and* $T_R(\lambda)$ are the reference spectrum in decibel and percentage terms, respectively. The relative transmission spectra of the 3.8° STFBG in various RI solutions were calculated with the transmission spectrum at an SRI of 1.4578 used as the reference. The results are shown in Fig. 4(b). Finally, we introduce the idea of the cladding mode resonance CW and a threshold value to identify it (for example, 0.3 dB). The CW is defined as the first wavelength on the short wavelength side where the relative transmission intensity is equal to the threshold value. It can be directly obtained by searching the first intersection on the short wavelength side of the relative transmission spectrum and the threshold line, as shown in Fig. 4(b). In addition, as the amplitudes of the cladding mode resonances gradually decrease with the increasing SRI, the CW shifts toward the longer wavelength side. Therefore, its variations in response to SRI changes can be used for SRI sensing. Note that when the temperature is fluctuated during the SRI measurement, which results in the shift of resonance wavelengths of the TFBG Bragg and cladding modes. In addition, the measured transmission spectra shift relative to the reference spectrum (as evidenced by the mismatch between their Bragg wavelengths). However, the Bragg wavelength is insensitive to the SRI, and the differential shift between the Bragg wavelength and cladding mode resonance wavelengths that results from temperature changes can be negligible.[16,20] Thus, the influence of temperature fluctuations can be eliminated by the calculating process of the relative transmission spectra as below. First, the measured transmission spectra are shifted relative to the reference spectrum such that their Bragg wavelengths coincide precisely. Then, the temperature-insensitive relative transmission spectra can be obtained by subtracting the reference spectrum from the aligned transmission spectra. As a result, the CW variations in response to SRI changes are insensitive to temperature.

Variations in the relative transmission spectra of the 3.8° STFBG in various RI solutions are shown in Fig. 5(a). When the SRI is equal to 1.4532, the relative intensities of the cladding mode resonances are lower than 0.9 dB. Moreover, the threshold line is unable to monitor the cladding mode resonance variations when the relative intensities are all lower than the threshold value. Therefore, it is incapable of measuring an SRI that is equal to or greater than 1.4532 when the threshold value of 0.9 dB is selected. These results suggest that the RI sensing range of TFBGs decreases as the threshold value increases. Figure 5(b) shows the CW responses of the 3.8° STFBG as functions of the RI of the glycerin solution measured at 589.3 nm with the threshold value of 0.1 dB, 0.3 dB, and 0.9 dB, respectively. The CW RI responses are non-linear. When the threshold value is 0.9 dB, the CW RI response is highly linear with a sensitivity of 464.2 nm/RIU in the 1.4258–1.4485 RI range and is similar to that of the method based cut-off mode.[13,18] As shown in Fig. 5(a), the CW position is near to the cut-off mode when the threshold value is 0.9 dB. Hence, the RI response in this case can be attributed to linear jumping of the CW from one cladding mode resonance to the next as the SRI increases. Clearly, the RI sensitivity is low (∼16 nm/RIU) in the 1.4125–1.4258 RI range. This is because the CW is kept at the same cladding mode in this RI variation range, and the CW change occurs due to a slight shift in resonance

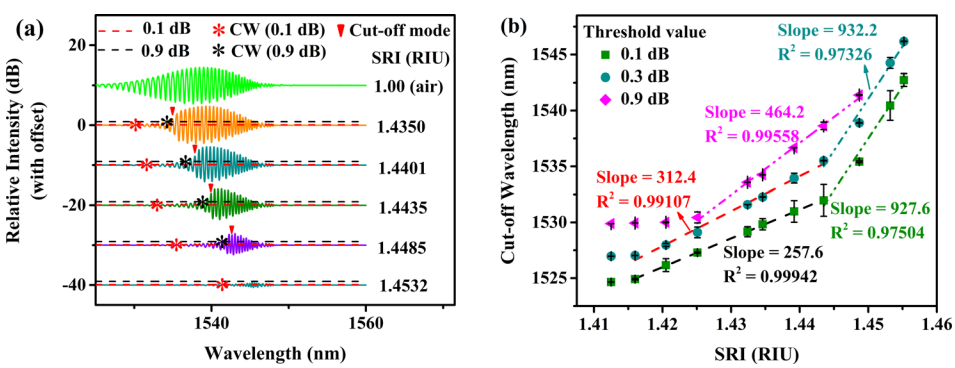

FIG. 5. (a) Variations in the 3.8° STFBG relative transmission spectra in various RI solutions. The CW and cut-off mode are marked by asterisks and triangles, respectively. (b) The cut-off wavelength responses of the 3.8° STFBG as functions of the refractive index of the glycerin solution at 589.3 nm when the threshold values are 0.1 dB, 0.3 dB, and 0.9 dB, respectively. The error bars are based on the results of three measurements.

wavelength of that cladding mode. The CW RI responses with the threshold values of 0.1 dB and 0.3 dB are similar. The RI range with a high-sensitivity response can be divided into two sections, and the linearity of each section is relatively high. When the threshold value is 0.1 dB, the RI sensitivity is 257.6 nm/RIU in the 1.4160–1.4435 RI range. This increases to 927.6 nm/RIU in the 1.4435–1.4552 RI range. The RI sensitivity transition point occurs at an SRI of 1.4435. If we use the wavelength of the cut-off mode at an SRI of 1.4435 as a reference wavelength, the relative intensities in air (RI ~1.00) of cladding mode resonances increase monotonically from the short wavelength side to the reference wavelength. When these cladding modes are affected by the SRI, the sensitivity of the RI response is relatively low. From the reference wavelength to the longer wavelength side, the relative intensities of the cladding mode resonances (measured in air) decrease monotonically. When these cladding modes are affected by the SRI, the sensitivity of the RI response is significantly enhanced, as shown in Figs. 5(a) and 5(b). One possible explanation for the difference in RI responses and the RI sensitivity enhancements is that our new demodulation method can be considered an absolute-discrimination method. The RI response of the "cut-off wavelength" may be affected not only by the selected threshold value but also by the resonance intensities of the cladding mode resonances or even the envelope of the cladding mode resonances.

TFBGs may have different cladding mode resonance intensities when they have different lengths, refractive index modulations, and other parameters.[22] Hence, the threshold values should be reconsidered for TFBGs with different cladding mode resonance intensities. In order to simplify the selection of the threshold value for all TFBGs, we propose a scheme to normalize the relative transmission spectra and the threshold value. For instance, the relative transmission spectra of the 3.8° STFBG in various RI solutions and the threshold value of 0.3 dB were normalized. From the calculation of the relative transmission spectrum in decibel term which is given by Eq. (1), the corresponding relative transmittivity spectra $\frac{T_M}{T_R}(\lambda)$ were calculated from the data in Fig. 4(b). The results are shown in Fig. 6(a).

The maximum of relative transmittivity in the air $\frac{T_{M\_air}}{T_R}(\lambda)$ marked by the red triangle is used to normalize all of the measured relative transmittivity spectra and threshold value. Their equations can be given as

$$T_{Normal}(\lambda) = \frac{\frac{T_M}{T_R}(\lambda) - 1}{Max\left[\frac{T_{M\_air}}{T_R}(\lambda)\right] - 1}, \tag{2}$$

$$V_{N,th} = \frac{10^{0.1\,V_{th}} - 1}{Max\left[\frac{T_{M\_air}}{T_R}(\lambda)\right] - 1}, \tag{3}$$

where $T_{Normal}(\lambda)$, V_{th}, and V_{N_th} are the normalized relative transmission spectrum, the threshold value, and the normalized threshold value, respectively. The relative transmission spectra of the 3.8° STFBG in various RI solutions and threshold value of 0.3 dB were individually normalized using the above equations, and the results are shown in Fig. 6(b).The cut-off wavelength of the 3.8° STFBG in these RI solutions is not changed after the normalizations.

C. RI responses of the PDTFBGs and STFBGs

In our SRI sensing experiments, the RI responses of the PDTFBGs and STFBGs were all measured three times using the calibrated aqueous glycerin solutions. Their relative transmission spectra were normalized using Eq. (2). Based on the resonance intensities of the TFBG cladding modes and the influence of the light source's stability on accuracy, a normalized threshold value of 0.04 (equal to 0.3 dB with the 3.8° STFBG) was selected to locate the cut-off wavelength of the TFBGs in various RI solutions. The cut-off wavelength RI responses of the 2.2°, 3.8° STFBGs, and 2.2°, 3.8° PDTFBG as functions of the RI of the glycerin solution at 589.3 nm are shown in Fig. 7(a).

As shown in Fig. 7(a), the RI sensing ranges of the 2.2° and 3.8° STFBGs are from 1.4350 to 1.4570 and from 1.4160 to 1.4552, respectively. The RI sensing range of 2.2°, 3.8°PDTFBG is from 1.3948 to 1.4570. It appears that the PDTFBG effectively enhances the RI sensing range compared to conventional STFBGs. The CW RI responses of 2.2°, 3.8° STFBGs and 2.2°, 3.8° PDTFBG are non-linear, but can all be divided into two approximately linear sections. The RI sensitivity of the 2.2° STFBG is 295.9 nm/RIU in the 1.4350–1.4485 RI range, but increases to 693.2 nm/RIU in the 1.4485–1.4570 RI range. The RI sensitivity of the 3.8° STFBG is 312.4 nm/RIU in the RI range of 1.4160–1.4435. It significantly increases to 932.2 nm/RIU in the 1.4435–1.4552 RI range. The RI sensitivity of the 2.2°, 3.8°

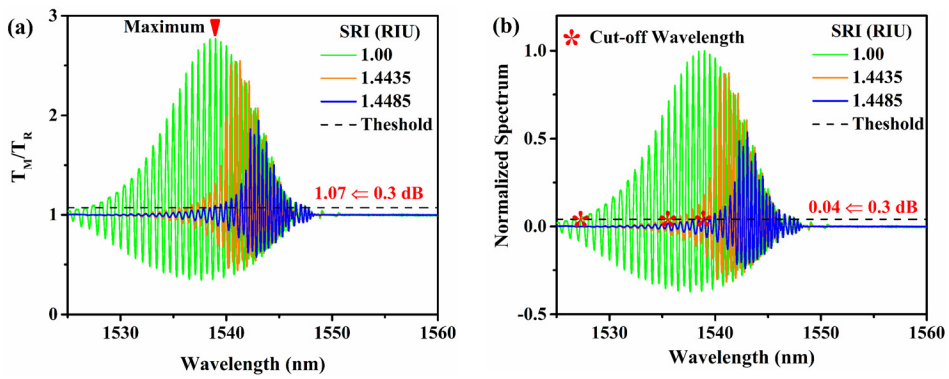

FIG. 6. The (a) absolute and (b) normalized relative transmittivity spectra of the 3.8° STFBG in various RI solutions. The maximum of relative transmittivity measured in air (RI ~1.00) is marked by a red triangle. The value of 0.04 represents normalization of the threshold value of 0.3 dB with the 3.8° STFBG.

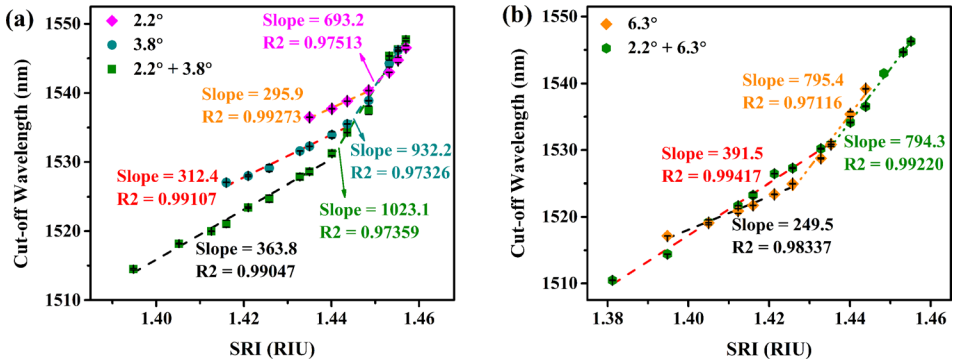

FIG. 7. (a) The CW responses of the 2.2° STFBG, 3.8° STFBG, and 2.2°, 3.8° PDTFBG, and (b) those of the 6.3° STFBG, and 2.2°, 6.3° PDTFBG as functions of the refractive index of the glycerin solution at 589.3 nm, respectively. The error bars are based on the results of three measurements.

PDTFBG is 363.8 nm/RIU in the 1.3948–1.4401 RI range. It reaches 1023.1 nm/RIU in the 1.4401–1.4570 RI range, which is double of the RI sensitivity when the demodulation method based cut-off mode is used.[18]

Moreover, another PDTFBG with tilt angles of 2.2° and 6.3° was fabricated. The CW RI responses this PDTFBG and the 6.3° STFBG are shown in Fig. 7(b). The normalized threshold value was also 0.04. The RI sensing range of the 6.3° STFBG is from 1.3948 to 1.4439. That of the 2.2°, 6.3° PDTFBG is from 1.3812 to 1.4552, which is even wider than the sum of RI sensing ranges of the 2.2° and 6.3° STFBGs. The CW RI responses of the 6.3° STFBG and 2.2°, 6.3° PDTFBG can also be divided into two approximately linear sections. The RI sensitivity of the 6.3° STFBG is 249.5 nm/RIU in the 1.3948–1.4258 RI range, but increases to 795.4 nm/RIU in the 1.4258–1.4439 RI range. The RI sensitivity of the 2.2°, 6.3° PDTFBG is 391.5 nm/RIU in the 1.3812–1.4350 RI range, and enhances to 794.3 in the 1.4350–1.4552 RI range.

From all results described above, it appears that the RI sensing range of TFBGs is effectively enlarged by using the PDTFBG. The RI sensing range of the PDTFBG can even be wider than the sum of the RI sensing ranges of two STFBGs, of which tilt angles are the same to each tilt angle of the PDTFBG, respectively. In addition, by using our proposed demodulation method, the RI sensitivities of the PDTFBG and STFBG are significantly enhanced in certain RI ranges.

When our proposed demodulation method is used in practical applications, two issues should be considered to improve the accuracy of the measured SRI. First, similar to the method based cut-off mode,[18] the high RI sensitivity obtained by using our demodulation method is also attributed to the transfer of the cut-off wavelength from one cladding mode resonance to an adjacent one as the SRI increases. Hence, our demodulation method is suitable for large SRI change measurements, and an SRI accuracy may be similar to that of the method based cut-off mode (10^{-3}). For tiny SRI changes, other methods can be applied such as monitoring individual resonances (closest to the cut-off mode resonance wavelength), which can achieve an SRI accuracy of about 2.5×10^{-5}.[18] Second, as our demodulation method is an absolute-discrimination method, the power fluctuation of the ASE light source could result in the deviations of the measured CW and SRI. This problem could be resolved by measuring the spectra of the light source simultaneously to obtain the deviation of the light source power, and then taking into account this deviation in the calculation of the relative transmission spectrum to eliminate the influence of the light source power instability.

IV. CONCLUSION

In this study, we proposed a demodulation method for RI sensing based on monitoring the variations in the TFBG cladding mode resonance "cut-off wavelength" in response to SRI changes. The "cut-off wavelength" can be identified by calculating the relative transmission spectra and using the threshold value. With our demodulation method, the RI sensitivities of TFBGs are significantly enhanced in certain RI ranges, and the temperature-induced cross sensitivity is eliminated. We also proposed and fabricated a PDTFBG that consisted of two parallel TFBGs. The RI sensing of the PDTFBG is much wider than those of conventional STFBGs. Its maximum RI sensitivity can reach 1023.1 nm/RIU in the 1.4401–1.4570 RI range when our proposed demodulation method is used.

ACKNOWLEDGMENTS

This work was supported by the National Key Research and Development Program of China (Grant No. 2017YFB1104600), the Suzhou Science and Technology Planning Project (Grant No. SYG201622), the Key research and development program of Shaanxi province (Grant No. 2017ZDXM-GY-120), the Fundamental Research Funds for the Central Universities (Grant No XJJ2016016), and the Program of the Collaborative Innovation Center of Suzhou Nano Science and Technology.

[1]G. Laffont and P. Ferdinand, Meas. Sci. Technol. **12**, 765 (2001).
[2]C. Chen, C. Caucheteur, P. Mégret, and J. Albert, Meas. Sci. Technol. **18**, 3117 (2007).
[3]T. Erdogan and J. E. Sipe, J. Opt. Soc. Am. A **13**, 296 (1996).
[4]L. Dong, B. Ortega, and L. Reekie, Appl. Opt. **37**, 5099 (1998).
[5]C. Caucheteur and P. Megret, IEEE Photonics Technol. Lett. **17**, 2703 (2005).
[6]C. Chen, Y. S. Yu, R. Yang, C. Wang, J. C. Guo, Y. Xue, Q. D. Chen, and H. B. Sun, J. Lightwave Technol. **31**, 455 (2013).
[7]X. Chen, K. Zhou, L. Zhang, and I. Bennion, IEEE Photonics Technol. Lett. **18**, 2596 (2006).
[8]N. J. Alberto, C. A. Marques, J. L. Pinto, and R. N. Nogueira, Appl. Opt. **49**, 6085 (2010).
[9]J. Albert, L. Y. Shao, and C. Caucheteur, Laser Photonics Rev. **7**, 83 (2013).
[10]Y. Wang, C. Shen, W. Lou, F. Shentu, C. Zhong, X. Dong, and L. Tong, Appl. Phys. Lett. **109**, 031107 (2016).

[11]A. C. L. Wong, W. H. Chung, H. Tam, and C. Lu, Opt. Exp. **19**, 409 (2011).
[12]B. Gu, W. Qi, J. Zheng, Y. Zhou, P. P. Shum, and F. Luan, Opt. Lett. **39**, 22 (2014).
[13]X. Chen, J. Xu, X. Zhang, T. Guo, and B. O. Guan, IEEE Photonics Technol. Lett. **29**, 719 (2017).
[14]W. Zhou, D. J. Mandia, S. T. Barry, and J. Albert, Opt. Lett. **40**, 1713 (2015).
[15]W. Zhou, Y. Zhou, and J. Albert, Laser Photonics Rev. **11**, 1600157 (2017).
[16]C. Chan, C. Chen, A. Jafari, A. Laronche, D. J. Thomson, and J. Albert, Appl. Opt. **46**, 1142 (2007).
[17]T. Guo, C. Chen, A. Laronche, and J. Albert, IEEE Photonics Technol. Lett. **20**, 635 (2008).
[18]Y. Lu, R. Geng, C. Wang, F. Zhang, C. Liu, T. Ning, and S. Jian, J. Lightwave Technol. **28**, 1677 (2010).
[19]T. Guo, F. Liu, B. Guan, and J. Albert, Opt. Laser Technol. **78**, 19 (2016).
[20]T. Wang, K. Liu, J. Jiang, M. Xue, P. Chang, and T. Liu, Opt. Express **25**, 14900 (2017).
[21]M. D. Baiad and R. Kashyap, Opt. Lett. **40**, 115 (2015).
[22]R. Wang, J. Si, T. Chen, L. Yan, H. Cao, X. Pham, and X. Hou, Opt. Express **25**, 23684 (2017).
[23]D. Feng, X. Gao, and J. Albert, Opt. Lett. **41**, 1201 (2016).